Indonesian Journal of Maritime Technology (ISMATECH)
Vol. 04, Issue 01, 2026
eISSN: 3025-518X
DOI: https://doi.org/10.35718/ismatech.v4i1.8481994

Energy Efficiency and Battery Load Sharing Analysis of 26-m Electric Supply Boat Using MATLAB

Atikah Rafiah[1*], Surya Hariyanto[1]
[1]Department of Marine Engineering, Faculty of Engineering, Hasanuddin University, Gowa, 92171, Indonesia

KEYWORDS
Battery load sharing;
Dual-bus architecture;
Electric supply boat;
Energy efficiency;
MATLAB
State of charge

ABSTRACT – Load division between parallel battery units in dual-bus battery-electric vessels directly governs current imbalance and battery degradation, yet design-stage quantification remains limited. This study evaluates three battery load sharing strategies for a 26-m electric supply boat with a 1,242 kWh LFP system under dual-bus DC architecture across five operating conditions using MATLAB with Coulomb counting and the Rint model. Power demand peaked at 644.31 kW at Transit 12 knots, where propulsion consumed 93.1% of the total energy budget. The optimal strategy achieved 0.0% load imbalance in four of five conditions against a static maximum of 8.2%, reducing the Joule loss index by 0.06% to 485,596 A^2. The SOC-adaptive strategy worsened imbalance at Transit 12 knots from 1.5% to 7.8%, confirming that gradient-based shifting is structurally unsuitable for dual-bus battery-only vessels. Terminal voltage analysis identified the DC bus threshold as the binding operational constraint during full-load transit rather than the BMS protection limit, a finding with direct implications for load shedding procedure design in comparable all-electric workboats.

*Corresponding Author | Atikah Rafiah | ✉ (atikahrafiah3@gmail.com)

INTRODUCTION

Every tonne of cargo moved by a nearshore supply boat leaves an emissions footprint that regulators are no longer willing to overlook. The International Maritime Organization (IMO) responded to this pressure through a sequence of binding instruments: the Energy Efficiency Design Index (EEDI) under MARPOL Annex VI, followed by the Energy Efficiency Existing Ship Index (EEXI) and the Carbon Intensity Indicator (CII), each imposing progressively stricter limits on carbon output per unit of transport work performed [1]. Against this backdrop, battery-electric propulsion has moved from demonstration projects to commercial orders. Over 400 hybrid and battery-electric vessels were on order globally as of recent industry counts, a figure that reflects not just regulatory compliance but a growing operator conviction that shore-charged energy storage is operationally viable for vessels with bounded, repeatable routes [2].

All-electric vessels resolve the combustion problem entirely but introduce a different class of engineering challenge. A battery energy storage system (BESS) cannot be replenished at sea, which means every allocation decision made at the design stage, including how much capacity to install, how to divide load across parallel battery units, and what discharge rate to permit, is locked in until the next drydock. Operational records from over 750 commercial marine BESS deployments show that equivalent full cycle counts in service fall consistently below designed values, and that load management strategy is one of the few variables within the operator's control that meaningfully affects how far short they fall [3]. Getting the energy distribution right at the design stage is therefore not an optimization exercise but a precondition for the vessel meeting its declared mission [4]. For vessels with dual-bus DC architecture, this challenge is compounded by a structural current asymmetry that no amount of total capacity can resolve without deliberate load allocation.

The dual-bus DC architecture common to small electric workboats assigns two independent ESS units to separate bus sections. One ESS serves the port-side propulsion motor and Bus A auxiliaries, while the other serves the starboard motor and Bus B auxiliaries. The topology satisfies classification society redundancy requirements and offers the efficiency advantages of DC distribution over conventional AC systems, including elimination of reactive power losses, direct compatibility with battery inverters, and inherent suitability for multi-string ESS integration [5], [6]. Its structural limitation is that Bus A and Bus B auxiliary loads are fixed by equipment assignment and are rarely equal, producing a persistent current imbalance that accelerates degradation on the more heavily loaded side and erodes the redundancy margin the topology was designed to preserve [7].

Research on shipboard power management has addressed this class of problem with increasing sophistication, though largely on vessels and configurations that differ from a small battery-only supply boat. A comprehensive DC power system framework was constructed for a pure electric propulsion vessel [7], but dynamic load imbalance between parallel ESS units across a defined mission cycle was not analyzed. A SOC-based power distribution strategy for parallel ESS in all-electric ships has been proposed [8], though its

applicability is limited to heterogeneous battery-supercapacitor systems. A power management architecture for an all-electric cargo vessel drawing on three parallel energy sources was proposed [9], a degree of freedom absent from a single-chemistry BESS system. Model predictive control was demonstrated for a hybrid DC shipboard system [10], but the control structure depends on a generator reference signal that does not exist in a fully battery-electric vessel. Decentralized power sharing through frequency decoupling was achieved for a fuel cell-battery DC system [11], a method equally dependent on source heterogeneity. Powertrain efficiency was benchmarked across multiple all-electric ship architectures [12], though at the system level rather than examining current distribution between parallel ESS units. An environmentally constrained power dispatch framework was proposed for fully electrified vessels [13], though the scope addressed fleet-level load scheduling rather than intra-ESS current balancing between parallel bus sections. However, no previous study has reported a design-stage load sharing analysis for a small, single-chemistry, battery-only supply boat under dual-bus DC architecture, leaving a gap relevant to the growing battery-electric workboat fleet.

Auxiliary load optimization at the design stage has been shown to produce measurable efficiency gains on vessels of comparable scale [14], and alternative energy implementation on Indonesian vessels has been demonstrated, including solar cells on traditional tourist ships [15] and LED-based electrical load planning on fishing vessels [16] and pioneer ships [17]. However, existing frameworks are structurally dependent on multiple heterogeneous power sources, with control structures built around diesel generator reference signals absent in a fully battery-electric vessel. These structural dependencies leave a specific gap for small, battery-only supply boats, where no dynamic voltage source exists to compensate for current asymmetry between parallel ESS units, and operational simplicity at commissioning favors a precalculated correction over strategies requiring continuous sensor feedback [18].

This paper presents a design-stage energy efficiency and battery load sharing analysis of a 26-m electric supply boat equipped with a 1,242 kWh lithium iron phosphate (LFP) BESS split across two independent 621 kWh ESS units at 750 VDC. Three load sharing strategies are derived and evaluated across five operating conditions defined in the Electrical Load Analysis: a static 50:50 split, a State of Charge (SOC)-adaptive heuristic, and a closed-form optimal strategy minimizing Joule loss. SOC depletion and terminal voltage are simulated in MATLAB using Coulomb counting with the Rint model. The study contributes quantitative load imbalance and Joule loss metrics across all operating conditions, identifies the binding voltage constraint during full-load transit, and establishes a replicable methodology for energy management assessment in comparable dual-bus electric supply boat designs.

METHODS

Research Object

The research object is a 26-m electric supply boat classed by an international classification society. Its principal particulars, sourced from the General Arrangement (GA) document, are summarized in Table 1.

Table 1. Principal Particulars of the 26-m Electric Supply Boat

Parameter	Value
Length Overall (LOA)	26.09 m
Breadth (B)	6.39 m
Depth (D)	3.00 m
Design Draught (T)	1.62 m
Maximum Speed	12 knots
Cargo Area	60 pallets / 40 MT
Complement	2 crew + 12 passengers

Seven approved shipyard engineering documents form the exclusive data source for the electrical system parameters and load profiles: General Arrangement (GA), Electrical Load Analysis (ELA), Electrical System Single Line Diagram (SLD), Power System Diagram, Battery System Specification, System Overview for Electric Propulsion System, and Hazard Identification (HAZID) Risk Assessment. No physical measurements, sea trial data, or manufacturer test results were used. The power flow model of the vessel's dual-bus DC architecture and the corresponding scope output under static load sharing are presented in Figure 1 and Figure 2 respectively.

The employment of verified shipyard engineering documents offers a dependable foundation for assessing the electrical functionality of the 26-meter electric supply vessel during its design phase. This method, grounded in documentation, allows for a structured evaluation of how battery loads are shared, the nature of power distribution, and energy efficiency in typical operational situations, all while avoiding the ambiguities linked to on-site measurements. In addition, the MATLAB model created aids in recognizing possible power disparities and helps enhance battery usage strategies, ultimately leading to greater system reliability and operational effectiveness.

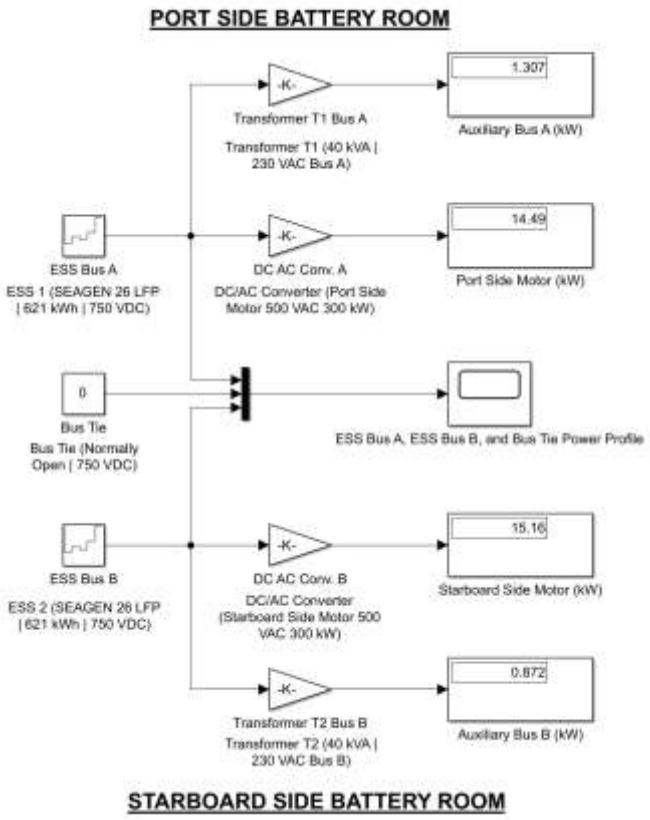

Figure 1. MATLAB/Simulink Power Flow Model of the 26-m Electric Supply Boat

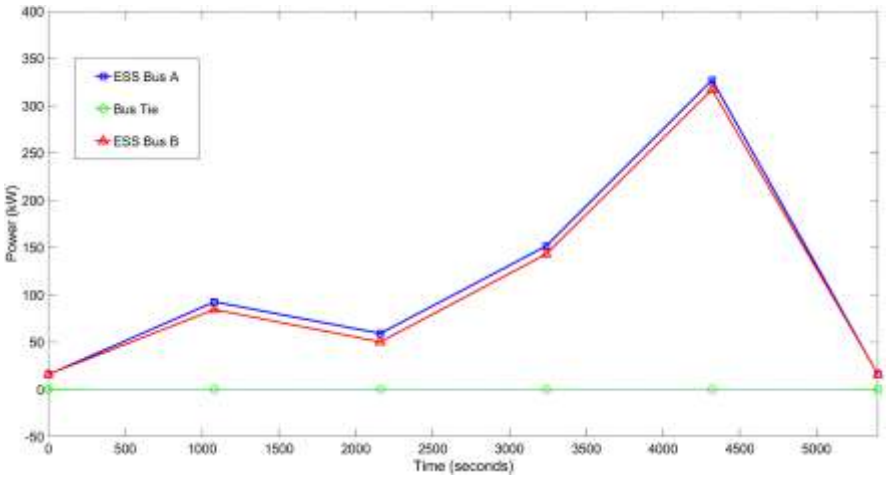

Figure 2. Simulink Scope Output: ESS Bus A, Bus B, and Bus Tie Power Profile Under Static Load Sharing Strategy

Figure 1 illustrates the Simulink model with two 621 kWh ESS units at 750 VDC, two 300 kW propulsion motor branches, 40 kVA auxiliary transformers, and a Normally Open Bus Tie. Figure 2 shows the corresponding scope output under static 50:50 load sharing across all five conditions, confirming independent bus operation with Bus Tie power flow at 0 kW throughout.

System Parameters and Variables

The energy storage system consists of two independent ESS units, one in the port-side (PS) battery room and one in the starboard (SB) battery room, each built from three parallel strings of eight series-connected lithium iron phosphate (LFP) modules. Each module is rated at 96 VDC and 270 Ah, giving a string voltage of 768 VDC and 207.36 kWh per string. Total installed capacity is 1,242 kWh at 750 VDC, equivalent to 829 Ah per ESS at bus level. All battery parameters are summarized in Table 2.

Table 2. Battery System Parameters of the LFP ESS

Parameter	Value	Source
Rated voltage per module	96 VDC	Battery Specification
Rated capacity per module	270 Ah	Battery Specification
Modules per string	8	Battery Specification
Strings per ESS	3	Single Line Diagram
ESS units	2 (PS + SB)	Single Line Diagram
DC bus voltage	750 VDC	Single Line Diagram
Total nominal capacity	1,242 kWh	Electrical Load Analysis
Equivalent capacity per ESS	829 Ah	Derived
Internal resistance per ESS	88.9 mΩ	Derived
BMS cutoff charge voltage	105 V/module	Hazard Identification (HAZID) Risk Assessment
BMS cutoff discharge voltage	87 V/module	Hazard Identification (HAZID) Risk Assessment
BMS usable SOC window	52.2% of physical range	Derived
Design C-rate limit	0.7C	Single Line Diagram
C-rate margin vs physical 1C	28.3%	Derived
Max operating temperature	55 °C	Hazard Identification (HAZID) Risk Assessment

Internal resistance per module is estimated from the BMS voltage swing endpoints as a conservative upper bound approximation, consistent with the approach described in [4] for design-stage analysis in the absence of Hybrid Pulse Power Characterization (HPPC) test data:

$$R_m = \frac{V_m - V_{co,d}}{I_{rated}} = \frac{96 - 87}{270} = 33.3\ \text{m}\Omega/\text{module} \quad (1)$$

where R_m is the internal resistance per module (mΩ), V_m is the nominal module voltage (V), $V_{co,d}$ is the BMS discharge cutoff voltage per module (V), and I_{rated} is the rated discharge current at 1C per module **(A)**, numerically equal to the rated capacity of 270 (Ah).

ESS-level resistance is then derived from the series-level parallel string configuration:

$$R_{ESS} = \frac{n_m \times R_m}{n_s} = \frac{8 \times 33.33}{3} = 88.9\ \text{m}\Omega/\text{ESS} \quad (2)$$

where R_{ESS} is the total internal resistance per ESS unit (mΩ), n_m is the number of modules per string, and n_s is the number of parallel strings per ESS.

The varied parameter across the study is propulsion load allocation between ESS Bus A and ESS Bus B, evaluated at five operating conditions from the ELA: Harbour, Departure/Arrival, Transit 8 knots, Transit 10 knots, and Transit 12 knots.

Load Sharing Strategies

Three strategies are formulated and compared. Each is described below with its governing equation, physical basis, and known limitation.

Strategy 1: Static 50:50. Propulsion power is divided equally between both buses. Each bus additionally carries its own fixed auxiliary load, half the chiller load, and half the 24 VDC switchboard load. Bus A and Bus B allocations are:

$$L_A = \frac{P_p}{2} + P_A + \frac{P_C}{2} + \frac{P_{24}}{2} \quad (3)$$

$$L_B = \frac{P_p}{2} + P_B + \frac{P_C}{2} + \frac{P_{24}}{2} \quad (4)$$

where L_A and L_B are the total load on Bus A and Bus B respectively (kW), P_p is total propulsion power (kW), P_A and P_B are the fixed auxiliary loads on Bus A and Bus B respectively (kW), P_c is the total battery chiller load (kW), and P_{24} is the 24 VDC switchboard load (kW).

Discharge current per bus is:

$$I = \frac{L \times 1000}{V_{bus}} \quad (5)$$

where I is the discharge current (A), L is the bus load (kW), and V_{bus} is the DC bus voltage (750 V).

Voltage drop across the ESS internal resistance follows:

$$\Delta V = I \times R_{ESS} \tag{6}$$

where ΔV is the voltage drop at the ESS output (V).

This strategy, documented in the vessel's SLD as "automatic load sharing," is simple to implement but does not account for the fixed auxiliary asymmetry between Bus A and Bus B, producing a persistent current imbalance that worsens at low propulsion conditions [7].

Strategy 2: State of Charge (SOC) Adaptive. This strategy modifies the static allocation by shifting up to 10% of the per-bus propulsion share when the SOC difference between consecutive mission stages exceeds 5 percentage points. The SOC reference sequence from the ELA is 100% → 87% → 85% → 71% → 100%. It responds to the mission energy state without real-time sensor feedback, but the shift direction follows the SOC gradient rather than instantaneous bus load asymmetry, leading to non-optimal load redistribution when the two quantities conflict [10].

Strategy 3: Optimal Minimum Joule Loss. The objective is to minimize the total squared current index, which serves as a proxy for conduction loss and differential battery stress across both ESS units:

$$J = I_A^2 + I_B^2 \tag{7}$$

where J is the Joule loss index (A^2), I_A is the discharge current on Bus A (A), and I_B is the discharge current on Bus B (A).

This objective is subject to the power balance constraint $L_A + L_B = P_{total}$ and the redistribution bound $|shift| \leq P_p/2$. Setting the first-order optimality condition to zero yields a closed-form solution that does not require iterative computation:

$$shift_{opt} = \frac{L_{B,fix} - L_{A,fix}}{2} \tag{8}$$

where $shift_{opt}$ is the optimal propulsion load shift from Bus A to Bus B (kW), $L_{B,fix}$ is the total fixed non-propulsion load on Bus B (kW), and $L_{A,fix}$ is the total fixed non-propulsion load on Bus A (kW).

This strategy analytically guarantees current equalization and can be directly implemented as a static feedforward correction in the vessel energy management system, though it does not incorporate SOC feedback and cannot respond to mid-mission battery state divergence [10].

Dynamic SOC Simulation

SOC depletion is simulated using Coulomb counting combined with the Rint equivalent circuit model. The Rint model is selected based on the review in [4] for its low computational cost, straightforward parameterization from BMS documentation, and adequate accuracy at the C-rates observed in this study (0.03C to 0.53C), where polarization transients are negligible. Its known limitation of not capturing dynamic polarization resistance or SOC-dependent impedance variation is acknowledged [19].

Open circuit voltage per module is modelled as a linear function of SOC between the BMS protection thresholds:

$$V_{oc}(SOC) = V_{co,d} + \frac{SOC}{100} \times (V_{co,c} - V_{co,d}) \tag{9}$$

where V_{oc} is the open circuit voltage per module (V), SOC is the state of charge (%), $V_{co,d}$ = 87 V/module is the BMS discharge cutoff voltage, and $V_{co,c}$ = 105 V/module is the BMS charge cutoff voltage, both sourced from the Hazard Identification (HAZID) Risk Assessment.

Terminal voltage at the ESS output is then:

$$V_t = V_{oc} \times n_m - I \times R_{ESS} \tag{10}$$

where V_t is the ESS terminal voltage (V) and n_m = 8 is the number of modules per string.

SOC is updated at each one-second timestep via Coulomb counting:

$$SOC(t+1) = max\left(0, SOC(t) - \frac{I}{Ah_E \times 3600} \times 100\right) \tag{11}$$

where SOC(t) is the state of charge at timestep t (%), I is the discharge current (A), and Ah_E = 829 Ah is the equivalent ESS capacity at bus level.

Simulations are run for three conditions selected on the basis of having discrete duration and initial SOC values available in the ELA: Harbour (3,600 s, SOC_0 = 100%), Transit 8 knots (5,400 s, SOC_0 = 100%), and Transit 12 knots (3,600 s, SOC_0 = 85%). The initial SOC of 85% for the Transit 12 knots simulation represents the SOC after unloading in the ELA mission profile, representing a worst-case discharge scenario under maximum rated load. Departure/Arrival and Transit 10 knots are excluded from dynamic simulation as they represent transitional states without discrete mission durations in the ELA documentation. Model validation against ELA reference values is presented in Table 3.

Table 3. Model Validation: Simulated Final SOC vs Electrical Load Analysis Reference

Condition	SOC_0 (%)	Model Final SOC (%)	ELA Reference (%)	Error (%pt)	Deviation Source
Harbour	100.0	97.5	N/A	-	No ELA endpoint reference
Transit 8 knots	100.0	85.7	87.0	-1.3	Rint underestimation at partial discharge rate
Transit 12 knots	85.0	32.4	N/A	-	Continuous rated load assumption without mission-average ELA reference

Transit 8 knots shows an error of −1.3 percentage points against the ELA reference of 87.0%, confirming acceptable model accuracy for this condition. Transit 12 knots, simulated from 85.0% SOC under the maximum rated load of 644.31 kW, reaches a final SOC of 32.4% after one hour, consistent with the worst-case rated load assumption stated in Table 3 [4].

Transformer Loading

Transformer loading for T1 (Bus A, 40 kVA) and T2 (Bus B, 40 kVA) is calculated as a percentage of rated capacity at a power factor of 0.9, sourced from the Power System Diagram:

$$T_{loading}(\%) = \frac{P_{bus}}{PF \times kVA_{rated}} \times 100 \quad (12)$$

where $T_{loading}$ is the transformer loading percentage (%), P_{bus} is the total auxiliary bus load (kW), PF is the power factor (0.9), and kVA_{rated} is the transformer rated capacity (kVA).

RESULTS AND DISCUSSION

Power Demand Distribution

Total power demand spans an approximately twentyfold range across the five operating conditions, from 31.83 kW at Harbour to 644.31 kW at Transit 12 knots, as presented in Figure 3.

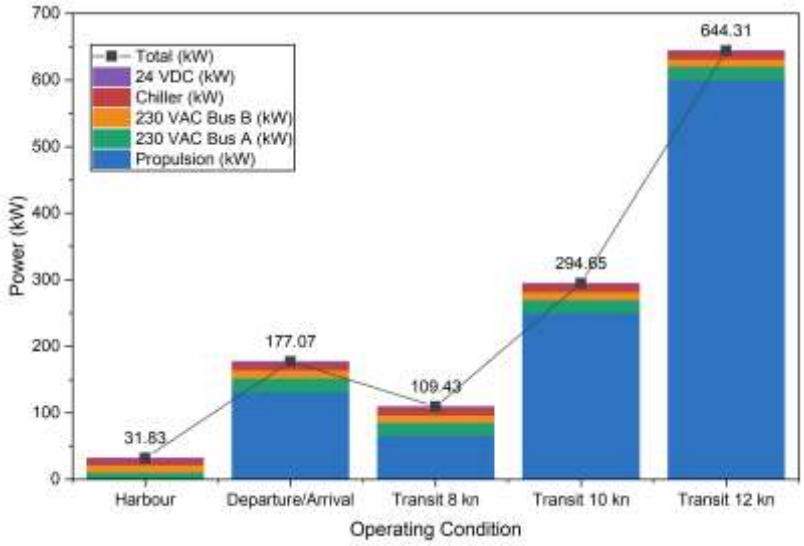

Figure 3. Power Demand Distribution Per Operating Condition

The dashed line in Figure 3 represents total demand with a 5% design margin, included as a reference for electrical system sizing. At Transit 12 knots, the 600 kW propulsion draw alone consumes 93.1% of the total energy budget, compressing the auxiliary share to just 44.31 kW combined across both buses. This extreme propulsion dominance has a direct consequence for load sharing: any strategy that splits propulsion equally between two buses will produce nearly equal total bus loads regardless of auxiliary asymmetry, which explains why static imbalance at maximum speed is only 1.5% despite the structural gap in auxiliary assignment.

The intermediate and low-speed conditions tell a different story. At Harbour propulsion is absent and all 31.83 kW is drawn by auxiliaries including HVAC, cooling pumps, battery chillers, and navigation systems, making it the sole condition where auxiliary loads constitute 100% of demand. The fixed difference between Bus A auxiliaries (10.93 kW) and Bus B auxiliaries (11.15 kW) is small at this condition, producing minimal imbalance of 0.7%. Transit 8 knots represents the most challenging condition for load sharing: with only 66 kW propulsion (60.3% of total 109.43 kW), the small propulsion split of 33 kW per bus is insufficient to dilute the auxiliary asymmetry, producing the highest static imbalance of 8.2%. The stable auxiliary baseline of 43.43 to 45.07 kW across all propulsion-active conditions confirms that hotel and service loads are structurally constant, which any load sharing strategy must treat as fixed rather than optimizable.

Static and SOC-Adaptive Load Sharing

The load distribution between Bus A and Bus B under the static and SOC-adaptive strategies across all five conditions is presented in Figure 4, with the full numerical comparison consolidated in Table 4.

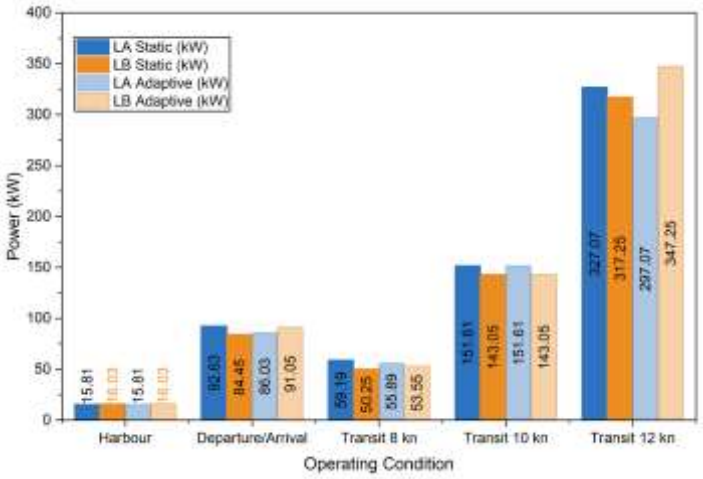

Figure 4. Static vs SOC-Adaptive Load Sharing ESS Bus A and Bus B

The persistent Bus A surplus under the static strategy traces directly to the fixed auxiliary load gap between Bus A and Bus B, which ranges from 8.18 to 9.82 kW across propulsion-active conditions. The most pronounced static imbalance occurs at Transit 8 knots, reaching 8.2% with Bus A carrying 59.19 kW against Bus B at 50.24 kW. At Departure/Arrival, static imbalance reaches 4.6%, while at Transit 10 knots it is 2.9%. At Transit 12 knots, the large 600 kW propulsion allocation reduces the relative effect of the auxiliary load gap, reducing static imbalance to only 1.5%. This inverse relationship between propulsion magnitude and imbalance severity confirms that load sharing strategies have the greatest impact on battery stress at intermediate speed conditions rather than at maximum rated load. Voltage drop across the ESS internal resistance at Bus A ranges from 1.87 V at Harbour to 38.76 V at Transit 12 knots, reflecting the direct proportionality between discharge current and resistive drop established in equation (6).

The SOC-adaptive strategy produces mixed results across the five conditions. At Harbour, the shift maintains imbalance at 0.7%. At Departure/Arrival and Transit 8 knots, the shift improves imbalance from 4.6% to 2.8% and from 8.2% to 2.1% respectively, demonstrating that gradient-based correction is effective when the SOC gradient aligns with the direction of bus asymmetry. However, at Transit 12 knots the identical shift direction worsens imbalance from 1.5% to 7.8%, because the propulsion share transferred to Bus B amplifies rather than corrects the existing asymmetry at that load level. At Transit 10 knots, the SOC gradient falls below the 5-point activation threshold, leaving the allocation unchanged from the static baseline at 2.9%. This pattern reveals a structural limitation: the SOC gradient at affected mission stages sometimes points away from the instantaneous bus asymmetry, and the strategy has no mechanism to detect this conflict. The behavior is not caused by parameter tuning but by the inherent incompatibility of single-signal open-loop heuristics applied to two-

variable allocation problems, consistent with findings in [10] and with evidence that unreasonable power distribution in parallel ESS units accelerates degradation of lower-SOC units [8].

The full numerical comparison across all conditions is presented in Table 4.

Table 4. Summary of Load Sharing Results Across All Operating Conditions

Parameter	Harbour	Departure/Arrival	Transit 8 kn	Transit 10 kn	Transit 12 kn
P_{total} (kW)	31.83	177.07	109.43	294.65	644.31
ESS-A Static (kW)	15.80	92.62	59.19	151.60	327.06
ESS-B Static (kW)	16.03	84.45	50.24	143.04	317.25
Share-A Static (%)	49.7	52.3	54.1	51.5	50.8
Share-A Adaptive (%)	49.7	48.6	51.1	51.5	46.1
Share-A Optimal (%)	49.7	50.0	50.0	50.0	50.0
Voltage Drop Bus A (V)	1.87	10.98	7.01	17.97	38.76
Imbalance Static (%)	0.7	4.6	8.2	2.9	1.5
Imbalance Adaptive (%)	0.7	2.8	2.1	2.9	7.8
Imbalance Optimal (%)	0.7	0.0	0.0	0.0	0.0
T1 Loading (%)	30.4	56.6	55.4	56.6	57.9
T2 Loading (%)	31.0	33.9	30.6	32.8	30.6

State of Charge Mission Profile

The ESS SOC trajectory through the complete mission cycle as recorded in the ELA is presented in Figure 5.

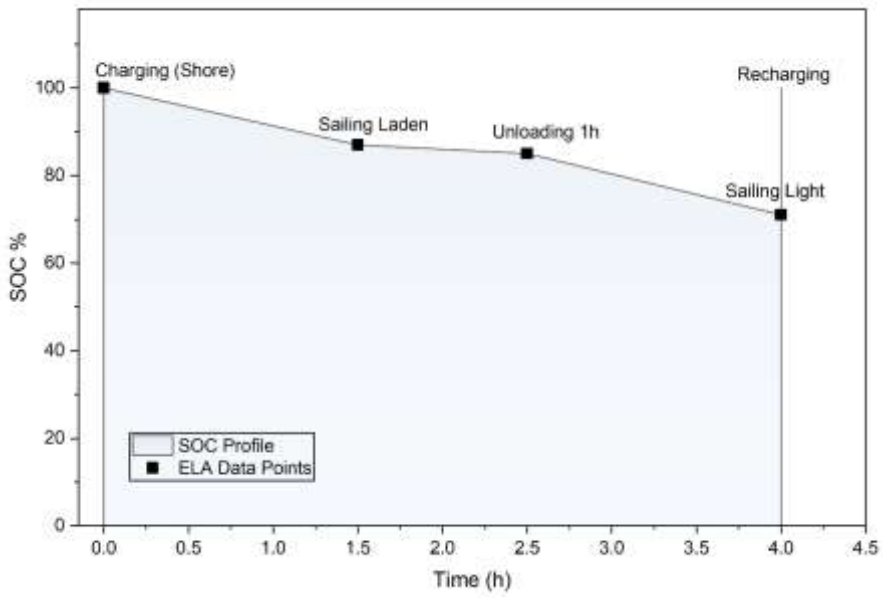

Figure 5. ESS State of Charge Mission Profile

Throughout the complete mission cycle, the ESS SOC follows a stepped depletion pattern that reflects the distinct energy intensity of each phase. Starting at 100%, SOC falls to 87% at the end of the laden outbound transit, dips further to 85% through the one-hour unloading phase, and reaches its lowest point of 71% at the end of the light return transit before shore recharging restores it to 100%. The 29 percentage point total drawdown across a complete round trip confirms that the installed capacity is well matched to the mission demand. The 71% minimum SOC sits 51 percentage points above the practical 20% depth of discharge limit, confirming that the 1,242 kWh installed capacity carries adequate margin for the declared mission without emergency reserve intervention. The BMS usable window of 52.2% of the physical cell range, bounded by 87 V/module discharge cutoff and 105 V/module charge cutoff, maintains a conservative safety margin consistent with established practice for marine LFP systems [2].

Dynamic State of Charge Simulation

Simulated SOC depletion curves for the three modelled conditions are presented in Figure 6, each reflecting a different combination of initial state and load intensity.

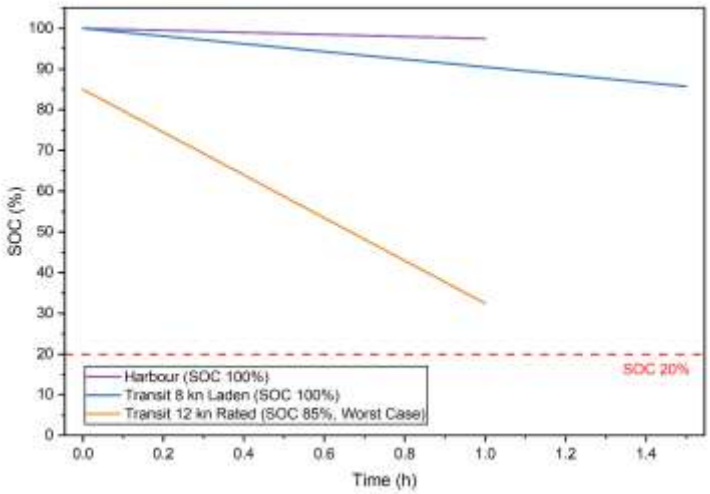

Figure 6. Dynamic State of Charge Simulation: Coulomb Counting and Rint Model

The Harbour curve declines gradually from 100% under 31.83 kW hotel load, reaching 97.5% after 3,600 seconds, consistent with the low energy draw of berthing operations. Transit 8 knots, simulated from 100% SOC under 109.43 kW load, reaches 85.7% after 5,400 seconds, showing a 1.3 percentage point error against the ELA reference of 87.0%, confirming acceptable model accuracy. The Rint model's known limitation of not capturing dynamic polarization resistance or SOC-dependent impedance variation is acknowledged [19], though this does not affect the comparative load sharing analysis which relies on steady-state current calculations.

Transit 12 knots presents the most severe case: simulated from 85.0% SOC under the maximum rated load of 644.31 kW, the steep depletion gradient reflects the high discharge rate at full propulsion demand, reaching a final SOC of 32.4% after 3,600 seconds. No ELA reference exists for this worst-case rated load condition, as the ELA mission profile records a time-averaged SOC of 71% at the end of the light return leg rather than a sustained rated load case. The load sharing comparison remains valid as it is based on steady-state current calculations independent of the dynamic SOC trajectory [4].

Terminal Voltage Analysis

ESS terminal voltage profiles across the three simulated conditions are presented in Figure 7, revealing a constraint boundary that is absent from hybrid vessel analysis.

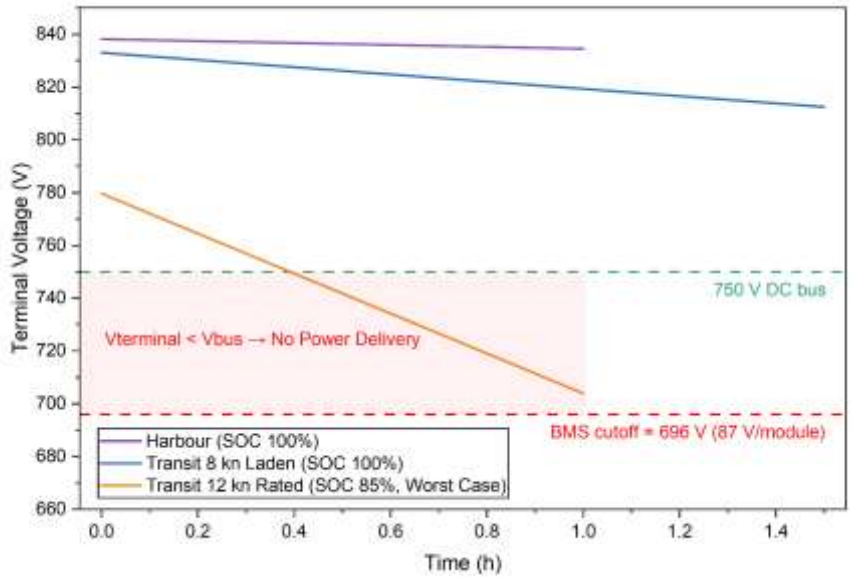

Figure 7. ESS Terminal Voltage Rint Model

Harbour and Transit 8 knots produce stable voltage trajectories well above both the 750 VDC bus threshold and the BMS discharge cutoff of 696 V (87 V/module x 8 modules), confirming that these conditions introduce no voltage constraint on ESS operation.

At Transit 12 knots, terminal voltage crosses below the 750 VDC bus threshold at approximately 0.5 hours into the simulation, before the BMS discharge cutoff is reached. This crossing point is operationally significant: once terminal voltage drops below bus voltage, the ESS cannot push current into the bus without active converter boosting or load shedding. The binding constraint at maximum speed transit is therefore the DC bus architecture, not the BMS cell protection. This voltage-limited discharge boundary is largely absent from hybrid vessel studies where a running generator holds the bus voltage reference [7], [10], and represents a constraint category unique to battery-only operation that must be explicitly addressed in the vessel's power management procedures and load shedding sequence.

Discharge C-Rate Analysis

Discharge current per ESS unit plotted against the three applicable current thresholds across all five operating conditions is presented in Figure 8.

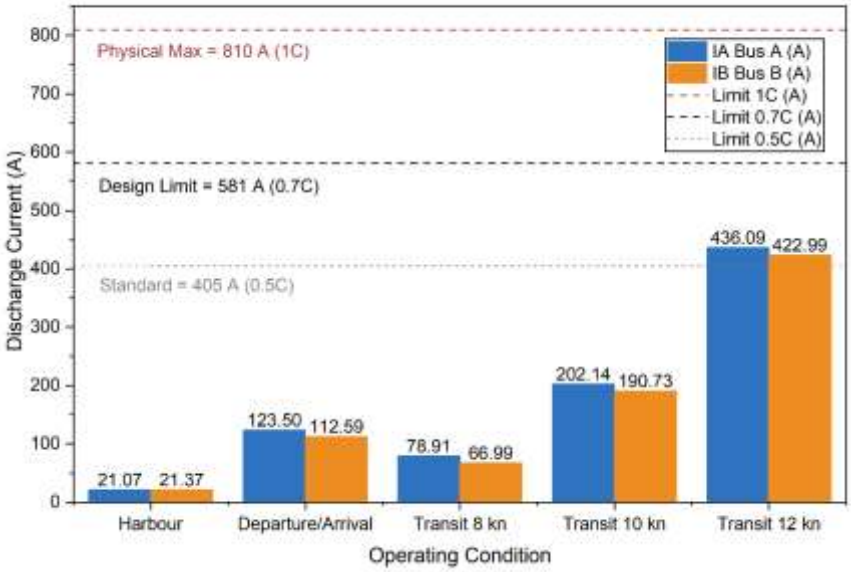

Figure 8. ESS Discharge Current vs C-Rate Limits

All operating conditions remain well within the design envelope defined by the standard 0.5C continuous rating (405 A), the 0.7C design limit from the SLD (580.6 A), and the physical 1C maximum (810 A). The peak current of 436 A on Bus A at Transit 12 knots corresponds to 0.53C, above the standard continuous rating but within the design boundary by a margin of 144.5 A. Three of five operating conditions fall below 0.15C, confirming that discharge rate stress is not the primary aging driver for this vessel class. The 28.3% gap between the 0.7C design limit and the 1C physical maximum provides the thermal headroom needed to sustain the highest demand condition without triggering BMS overcurrent protection. Conservative C-rate operation has been identified as a primary determinant of whether marine BESS installations achieve their designed equivalent full cycle count in service [3], reinforcing the practical value of maintaining this margin. This pattern also confirms that cycle depth management, rather than current magnitude, is the more consequential long-term battery health variable for this vessel class, making load sharing strategy the primary lever for extending ESS service life.

ESS Energy Balance

Remaining energy per ESS unit at each sequential mission stage under the static strategy is presented in Figure 9.

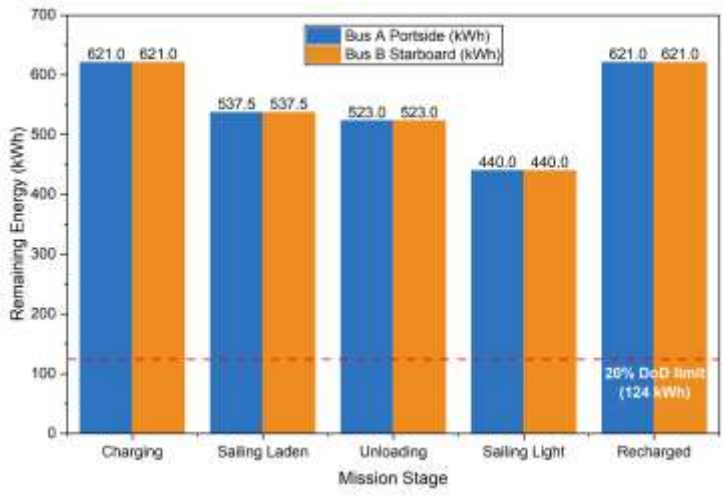

Figure 9. ESS Remaining Energy Per Mission Stage Bus A vs Bus B

Both ESS units draw energy at identical rates throughout the mission, a direct consequence of the 50:50 propulsion split combined with equal per-unit capacity of 621 kWh. The minimum per-unit reserve of 440 kWh at the Sailing Light stage is 3.5 times the practical minimum of 124 kWh per ESS at 20% depth of discharge, confirming that the vessel is not energy-capacity constrained for its declared mission. The symmetric trajectories of Bus A and Bus B across all five mission stages indicate that the static strategy does not introduce differential aging through energy imbalance at mission-stage resolution, though the current-level asymmetry documented in Table 4 persists within each stage. This distinction is important: energy balance at mission-stage resolution does not preclude current imbalance within individual operating conditions.

Load Sharing Strategy Comparison

Per-condition load imbalance across all three strategies is compared in Figure 10.

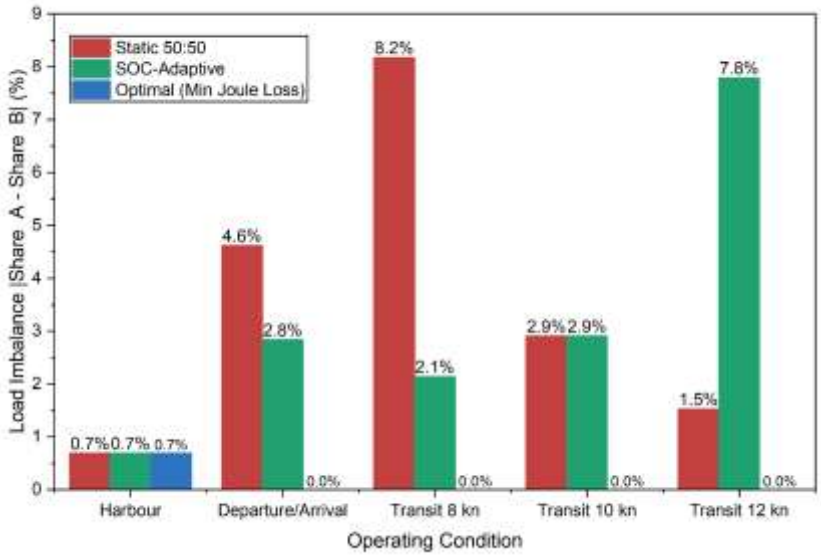

Figure 10. Load Sharing Imbalance Three Strategies Comparison

The performance gap between the three strategies is most visible at Transit 8 knots, where imbalance ranges from 8.2% under the static strategy, to 2.1% under SOC-adaptive, to 0.0% under the optimal strategy. The optimal strategy reaches 0.0% imbalance in four of five conditions, fully eliminating the pronounced asymmetry at Departure/Arrival, Transit 8 knots, Transit 10 knots, and Transit 12 knots. The residual 0.7% at Harbour is irreducible because propulsion is zero, leaving only the 0.22 kW fixed auxiliary difference as the sole source of asymmetry.

The Joule loss index and imbalance range across all three strategies are summarized in Table 5.

Table 5. Joule Loss Index Comparison Across Three Load Sharing Strategies

Strategy	Joule Loss Index (A^2)	Change vs Static	Imbalance Range (%)
Static 50:50	485,878	—	0.7 – 8.2
SOC-adaptive	487,927	+0.42%	0.7 – 7.8
Optimal (Min. Joule Loss)	485,596	−0.06%	0.0 – 0.7

The optimal strategy improves on the static baseline by 0.06%, while the SOC-adaptive strategy deteriorates it by 0.42%. The direction of SOC-adaptive deterioration is systematic rather than random, occurring specifically when the SOC gradient directs load toward the already heavier bus and revealing a structural incompatibility between gradient-based heuristics and fixed-asymmetry dual-bus topologies. The absolute Joule loss reduction is modest, but the consequential benefit lies in eliminating the persistent current asymmetry. Unbalanced utilization between parallel ESS units has been identified as one of the most consistent contributors to premature cycle life degradation in commercial marine BESS deployments [3]. An 8.2% current imbalance sustained across every Transit 8 knots condition compounds into a measurable aging differential over the vessel's service life, an outcome the optimal strategy eliminates at no additional hardware cost, requiring only a precalculated feedforward correction to the load setpoints in the power management system.

Energy Efficiency

The propulsion-to-auxiliary energy proportion per operating condition is presented in Figure 11.

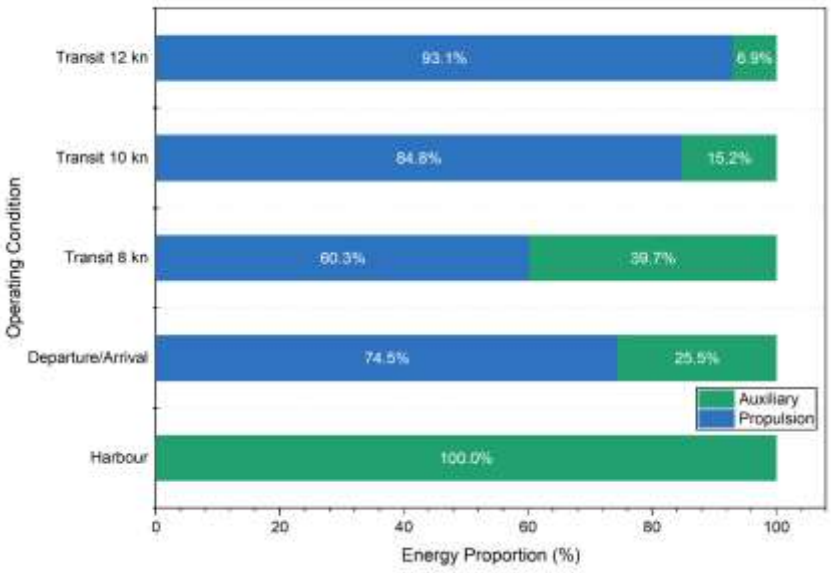

Figure 11. Energy Efficiency Propulsion vs Auxiliary Per Operating Condition

Two distinct efficiency regimes govern different segments of the operating envelope. At Transit 12 knots, the 93.1% propulsion share establishes that energy efficiency at maximum design speed is overwhelmingly governed by hull resistance and propulsion system performance, with auxiliary load management contributing less than 7% of the total energy budget and offering negligible efficiency leverage. At the opposite extreme, the 100% auxiliary fraction at Harbour makes hotel load management the sole efficiency lever, with battery chiller, HVAC, and navigation systems collectively drawing 31.83 kW during berthing. This finding is consistent with results for all-electric cargo vessels, where auxiliary loads during port operations were identified as a disproportionate contributor to total voyage energy consumption relative to their operational duration [9].

Static vs Optimal Load Sharing

Static and optimal power distributions placed side by side across all five conditions are presented in Figure 12.

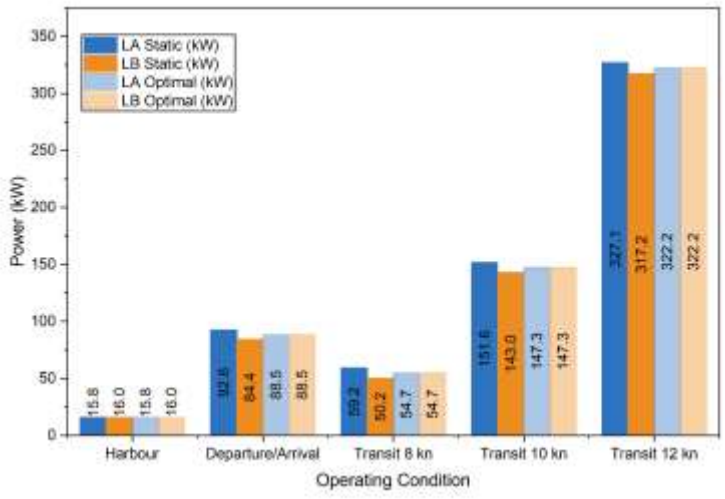

Figure 12. Static vs Optimal Load Sharing ESS Bus A and Bus B

The equalization is most visible at Departure/Arrival, Transit 8 knots, and Transit 10 knots, where the static strategy produces the most pronounced bar asymmetry between Bus A and Bus B. Under the optimal strategy, both bars reach equal height at every propulsion-active condition, achieved entirely through the precalculated shift derived from equation (8). The shift value is fixed by the SLD equipment assignment and does not change between voyages, does not require sensor feedback, and does not depend on battery state. This implementation simplicity provides a practical advantage over SOC-adaptive or model predictive approaches, both of which require continuous state monitoring and introduce the risk of counterproductive control actions when signal and system state diverge [10].

Transformer Loading

As shown in Table 4, transformer T1 on Bus A reaches its highest loading of 57.9% at Transit 12 knots, while transformer T2 on Bus B peaks at 33.9% at Departure/Arrival. Both remain within their 40 kVA rated capacity across all five conditions, confirming adequate transformer sizing. The consistently lower T2 loading reflects the structurally smaller Bus B auxiliary assignment. The available 66.1% loading headroom on T2 at the most demanding condition provides adequate margin for future Bus B consumer additions.

CONCLUSION

Three battery load sharing strategies were evaluated for a 26-m electric supply boat with a 1,242 kWh LFP BESS under dual-bus DC architecture across five operating conditions. Total power demand peaks at 644.31 kW at Transit 12 knots where propulsion accounts for 93.1% of the energy budget. The optimal strategy achieves 0.0% load imbalance in four of five conditions against a static maximum of 8.2%, reducing the Joule loss index by 0.06% to 485,596 A^2 through a precalculated feedforward correction requiring no additional hardware. The SOC-adaptive strategy worsens imbalance at Transit 12 knots from 1.5% to 7.8%, confirming that gradient-based shifting is unsuitable for dual-bus battery-only vessels. Terminal voltage analysis identifies the 750 VDC bus threshold as the binding operational constraint during maximum speed transit, which must be reflected in load shedding procedures. All discharge currents remain within the 0.7C design limit and the minimum SOC of 71% confirms adequate capacity for the declared mission. These results establish a replicable design-stage methodology for energy management assessment in all-electric workboats subject to CII requirements on bounded nearshore routes.

ACKNOWLEDGEMENT

The authors thank the shipyard for providing the engineering design documentation that forms the basis of this analysis. All documents were made available under confidentiality for academic research purposes.

REFERENCES

[1] H. P. Nguyen *et al.*, “The electric propulsion system as a green solution for management strategy of CO2 emission in ocean shipping: A comprehensive review,” *Int. Trans. Electr. Energy Syst.*, vol. 31, no. 11, pp. 1–29, 2020, doi: 10.1002/2050-7038.12580.

[2] M. Kolodziejski and I. Michalska-Pozoga, "Battery energy storage systems in ships' hybrid/electric propulsion systems," *Energies*, vol. 16, no. 3, p. 1122, 2023, doi: 10.3390/en16031122.

[3] W. He *et al.*, "Lessons learned from the commercial exploitation of marine battery energy storage systems," *J. Energy Storage*, vol. 87, p. 111440, 2024, doi: 10.1016/j.est.2024.111440.

[4] Y. Luo *et al.*, "Reviews on the power management for shipboard energy storage systems," *Sustain. Horizons*, vol. 9, p. 100094, 2024, doi: 10.1016/j.horiz.2024.100094.

[5] R. Prenc, A. Cuculić, and I. Baumgartner, "Advantages of using a DC power system on board ship," *J. Marit. Transp. Sci.*, vol. 52, no. 1, pp. 83–97, 2016, doi: 10.18048/2016.52.05.

[6] M. U. Mutarraf, Y. Terriche, K. A. K. Niazi, J. C. Vasquez, and J. M. Guerrero, "Energy storage systems for shipboard microgrids—A review," *Energies*, vol. 11, no. 12, p. 3492, 2018, doi: 10.3390/en11123492.

[7] Y. Kim, J. Kim, J. Jung, S. Kim, J. Choi, and H. Lee, "Comprehensive design of DC shipboard power systems for pure electric propulsion ship based on battery energy storage system," *Energies*, vol. 14, no. 17, p. 5264, 2021, doi: 10.3390/en14175264.

[8] Y. Liu, H. Wang, Q. Zhang, Y. Wen, W. Hu, and H. Zhang, "Power distribution strategy based on state of charge balance for hybrid energy storage systems in all-electric ships," *J. Power Electron.*, vol. 21, no. 8, pp. 1213–1224, 2021, doi: 10.1007/s43236-021-00267-z.

[9] D. Karkosiński, W. A. Rosiński, P. Deinrych, and S. Potrykus, "Onboard energy storage and power management systems for all-electric cargo vessel concept," *Energies*, vol. 14, no. 4, p. 1048, 2021, doi: 10.3390/en14041048.

[10] D. Park and M. Zadeh, "Modeling and predictive control of shipboard hybrid DC power systems," *IEEE Trans. Transp. Electrif.*, vol. 7, no. 2, pp. 892–904, 2020, doi: 10.1109/TTE.2020.3027184.

[11] T. Kopka, F. Mylonopoulos, A. Coraddu, and H. Polinder, "Decentralized power sharing with frequency decoupling for a fuel cell-battery DC shipboard power system," in *Proc. 4th Int. Conf. Modelling and Optimisation of Ship Energy Systems (MOSES 2023), Delft, Netherlands*, 2023. doi: 10.59490/moses.2023.670.

[12] P. Ghimire, M. Zadeh, J. Thorstensen, and E. Pedersen, "Data-driven efficiency modeling and analysis of all-electric ship powertrain: A comparison of power system architectures," *IEEE Trans. Transp. Electrif.*, vol. 8, no. 2, pp. 1930–1943, 2022, doi: 10.1109/TTE.2021.3123886.

[13] F. D. Kanellos, A. Anvari-Moghaddam, and J. M. Guerrero, "A cost-effective and emission-aware power management system for ships with integrated full electric propulsion," *Electr. Power Syst. Res.*, vol. 150, pp. 63–75, 2017, doi: 10.1016/j.epsr.2017.05.003.

[14] Suardi *et al.*, "Optimizing generator power usage through LED lighting distribution on tugboats: A case study of a 26.80-meter vessel," *Indones. J. Marit. Technol.*, vol. 3, no. 1, pp. 11–13, 2025, doi: 10.35718/ismatech.v3i1.1285.

[15] Suardi, M. K. Maulana, R. J. Ikhwani, M. U. Pawara, F. Mahmuddin, and M. Tasrief, "Design and implementation of solar cells as an alternative power source for pinisi ships," *Comput. Exp. Res. Mater. Renew. Energy*, vol. 7, no. 2, p. 93, 2024, doi: 10.19184/cerimre.v7i2.52111.

[16] Suardi, W. Setiawan, A. Y. Kyaw, N. Baya, and M. R. T, "Plan for the power requirements of the lights in the fishing boat room using LED lights," *Indones. J. Marit. Technol.*, vol. 1, no. 1, pp. 1–6, 2023, doi: 10.35718/ismatech.v1i1.877.

[17] G. Wati *et al.*, "Analysis of generator power requirements for lighting distribution using LED lights on a 500 DWT Sabuk Nusantara," *Indones. J. Marit. Technol.*, vol. 1, no. 2, pp. 45–51, 2023, doi: 10.35718/ismatech.v1i2.1038.

[18] K. Kwon, D. Park, and M. K. Zadeh, "Load frequency-based power management for shipboard DC hybrid power systems," in *Proc. 2020 IEEE 29th International Symposium on Industrial Electronics (ISIE), Delft, Netherlands*, 2020, pp. 142–147. doi: 10.1109/ISIE45063.2020.9152418.

[19] J. P. Roselyn, A. Ravi, D. Devaraj, and R. Venkatesan, "Optimal SoC estimation considering hysteresis effect for effective battery management in shipboard batteries," *IEEE J. Emerg. Sel. Top. Power Electron.*, vol. 9, no. 6, pp. 6777–6784, 2020, doi: 10.1109/JESTPE.2020.3034362.